symmetry

MDPI

Article

Numerical Simulation of Pattern Formation on Surfaces Using an Efficient Linear Second-Order Method

Hyun Geun Lee

Department of Mathematics, Kwangwoon University, Seoul 01897, Korea; leeh1@kw.ac.kr

Received: 4 June 2019; Accepted: 25 July 2019; Published: 5 August 2019

Abstract: We present an efficient linear second-order method for a Swift–Hohenberg (SH) type of a partial differential equation having quadratic-cubic nonlinearity on surfaces to simulate pattern formation on surfaces numerically. The equation is symmetric under a change of sign of the density field if there is no quadratic nonlinearity. We introduce a narrow band neighborhood of a surface and extend the equation on the surface to the narrow band domain. By applying a pseudo-Neumann boundary condition through the closest point, the Laplace–Beltrami operator can be replaced by the standard Laplacian operator. The equation on the narrow band domain is split into one linear and two nonlinear subequations, where the nonlinear subequations are independent of spatial derivatives and thus are ordinary differential equations and have closed-form solutions. Therefore, we only solve the linear subequation on the narrow band domain using the Crank–Nicolson method. Numerical experiments on various surfaces are given verifying the accuracy and efficiency of the proposed method.

Keywords: Swift–Hohenberg type of equation; surfaces; narrow band domain; closest point method; operator splitting method

1. Introduction

A Swift–Hohenberg (SH) type of partial differential equation [1] has been used to study pattern formation [2–5]:

$$\frac{\partial \phi}{\partial t} = -\left(\phi^3 - g\phi^2 + \left(-\epsilon + (1+\Delta)^2\right)\phi\right),$$

where ϕ is the density field and $g \geq 0$ and $\epsilon > 0$ are constants. In general, the equation does not have an analytical solution, thus various computational algorithms [6–13] have been proposed to obtain a numerical solution. However, most of them were solved on flat surfaces except [12,13].

In this paper, we present an efficient linear second-order method for the SH type of equation on surfaces, which is based on the closest point method [14,15]. We introduce a narrow band domain of a surface and apply a pseudo-Neumann boundary condition on the boundary of the narrow band domain through the closest point [16]. This results in a constant value of ϕ in the direction normal to the surface, thus the Laplace–Beltrami operator can be replaced by the standard Laplacian operator. In addition, we split the equation into one linear and two nonlinear subequations [17,18], where the nonlinear subequations are independent of spatial derivatives and thus are ordinary differential equations and have closed-form solutions. Therefore, we only solve the linear subequation on the narrow band domain using the Crank–Nicolson method. As a result, our method is easy to implement and linear.

This paper is organized as follows. In Section 2, we describe the SH type of equation on a narrow band domain. In Section 3, we propose an efficient linear second-order method for the equation on the narrow band domain. Numerical examples on various surfaces are given in Section 4. Finally, we conclude in Section 5.

2. Swift–Hohenberg Type of Equation on a Narrow Band Domain

The SH type of equation on a surface $\mathcal{S}$ is given by

$$\frac{\partial \phi(\mathbf{x},t)}{\partial t} = -\left(\phi^3(\mathbf{x},t) - g\phi^2(\mathbf{x},t) + \left(-\epsilon + (1+\Delta_{\mathcal{S}})^2\right)\phi(\mathbf{x},t)\right), \quad \mathbf{x} \in \mathcal{S},\ 0 < t \le T, \tag{1}$$

where $\Delta_{\mathcal{S}}$ is the Laplace–Beltrami operator [19,20]. Next, let $\Omega_\delta = \{\mathbf{y} |\ \mathbf{x} \in \mathcal{S}, \mathbf{y} = \mathbf{x} + \eta\mathbf{n}(\mathbf{x})$ for $|\eta| < \delta\}$ be a δ-neighborhood of $\mathcal{S}$, where $\mathbf{n}(\mathbf{x})$ is a unit normal vector at $\mathbf{x}$. Then, we extend the Equation (1) to the narrow band domain Ω_δ:

$$\frac{\partial \phi(\mathbf{x},t)}{\partial t} = -\left(\phi^3(\mathbf{x},t) - g\phi^2(\mathbf{x},t) + \left(-\epsilon + (1+\Delta_{\mathcal{S}})^2\right)\phi(\mathbf{x},t)\right), \quad \mathbf{x} \in \Omega_\delta,\ 0 < t \le T \tag{2}$$

with the pseudo-Neumann boundary condition on $\partial\Omega_\delta$:

$$\phi(\mathbf{x},t) = \phi(\mathrm{cp}(\mathbf{x}),t), \tag{3}$$

where $\mathrm{cp}(\mathbf{x})$ is a point on $\mathcal{S}$, which is closest to $\mathbf{x} \in \partial\Omega_\delta$ [14]. For a sufficiently small δ, ϕ is constant in the direction normal to the surface. Thus, the Laplace–Beltrami operator in Ω_δ can be replaced by the standard Laplacian operator [14], i.e.,

$$\frac{\partial \phi(\mathbf{x},t)}{\partial t} = -\left(\phi^3(\mathbf{x},t) - g\phi^2(\mathbf{x},t) + \left(-\epsilon + (1+\Delta)^2\right)\phi(\mathbf{x},t)\right), \quad \mathbf{x} \in \Omega_\delta,\ 0 < t \le T. \tag{4}$$

3. Numerical Method

In this section, we propose an efficient linear second-order method for solving Equation (4) with the boundary condition (3). We discretize Equation (4) in $\Omega = [-L_x/2, L_x/2] \times [-L_y/2, L_y/2] \times [-L_z/2, L_z/2]$ that includes Ω_δ. Let $h = L_x/N_x = L_y/N_y = L_z/N_z$ be the uniform grid size, where N_x, N_y, and N_z are positive integers. Let $\Omega^h = \{\mathbf{x}_{ijk} = (x_i, y_j, z_k) |\ x_i = -L_x/2 + ih, y_j = -L_y/2 + jh, z_k = -L_z/2 + kh$ for $0 \le i \le N_x, 0 \le j \le N_y, 0 \le k \le N_z\}$ be a discrete domain. Let ϕ^n_{ijk} be an approximation of $\phi(\mathbf{x}_{ijk}, n\Delta t)$, where Δt is the time step. Let $\Omega^h_\delta = \{\mathbf{x}_{ijk} | \, |\psi_{ijk}| < \delta\}$ be a discrete narrow band domain, where ψ is a signed distance function for the surface $\mathcal{S}$, and $\partial\Omega^h_\delta = \{\mathbf{x}_{ijk} |\ I_{ijk}|\nabla_h I_{ijk}| \neq 0\}$ are discrete domain boundary points, where $\nabla_h I_{ijk} = (I_{i+1,j,k} - I_{i-1,j,k}, I_{i,j+1,k} - I_{i,j-1,k}, I_{i,j,k+1} - I_{i,j,k-1})/(2h)$. Here, $I_{ijk} = 0$ if $\mathbf{x}_{ijk} \in \Omega^h_\delta$, and $I_{ijk} = 1$, otherwise.

We here split Equation (4) into the following subequations:

$$\frac{\partial \phi}{\partial t} = -(\phi^3 - \epsilon\phi), \tag{5}$$

$$\frac{\partial \phi}{\partial t} = g\phi^2, \tag{6}$$

$$\frac{\partial \phi}{\partial t} = -(1+\Delta)^2\phi. \tag{7}$$

Equations (5) and (6) are solved analytically and the solutions ϕ^{n+1}_{ijk} are given as follows:

$$\phi^{n+1}_{ijk} = \frac{\phi^n_{ijk}}{\sqrt{(\phi^n_{ijk})^2/\epsilon + (1 - (\phi^n_{ijk})^2/\epsilon)e^{-2\epsilon\Delta t}}} \quad \text{and} \quad \phi^{n+1}_{ijk} = \frac{\phi^n_{ijk}}{1 - g\Delta t\phi^n_{ijk}},$$

respectively. In addition, Equation (7) is solved using the Crank–Nicolson method:

$$\frac{\phi_{ijk}^{n+1} - \phi_{ijk}^{n}}{\Delta t} = -\frac{(1+\Delta_h)^2}{2}(\phi_{ijk}^{n+1} + \phi_{ijk}^{n}) \tag{8}$$

with the boundary condition on $\partial\Omega_\delta^h$:

$$\phi_{ijk}^{n} = \phi^n(\mathrm{cp}(\mathbf{x}_{ijk})).$$

Here, $\Delta_h\phi_{ijk} = (\phi_{i+1,j,k} + \phi_{i-1,j,k} + \phi_{i,j+1,k} + \phi_{i,j-1,k} + \phi_{i,j,k+1} + \phi_{i,j,k-1} - 6\phi_{ijk})/h^2$. The numerical closest point $\mathrm{cp}(\mathbf{x}_{ijk})$ for a point $\mathbf{x}_{ijk} \in \partial\Omega_\delta^h$ is defined as

$$\mathrm{cp}(\mathbf{x}_{ijk}) = \mathbf{x}_{ijk} - |\psi_{ijk}|\frac{\nabla_h|\psi_{ijk}|}{|\nabla_h|\psi_{ijk}||}.$$

In general, $\mathrm{cp}(\mathbf{x}_{ijk})$ is not a grid point in Ω_δ^h, i.e., $\mathrm{cp}(\mathbf{x}_{ijk}) \notin \Omega_\delta^h$, and thus we use trilinear interpolation and take $\delta > \sqrt{3}h$ to obtain $\phi(\mathrm{cp}(\mathbf{x}_{ijk}))$. The resulting implicit linear discrete system of Equation (8) is solved efficiently using the Jacobi iterative method. We iterate the Jacobi iteration until a discrete L^2-norm of the consecutive error on Ω_δ^h is less than a tolerance tol. Here, the discrete L^2-norm on Ω_δ^h is defined as $\|\phi\|_{L^2(\Omega_\delta^h)} = \sqrt{\sum_{\mathbf{x}_{ijk}\in\Omega_\delta^h}\phi_{ijk}^2/\#\Omega_\delta^h}$, where $\#\Omega_\delta^h$ is the cardinality of Ω_δ^h. Then, the second-order solution of Equation (4) is evolved by five stages [21]

$$\begin{aligned}
\phi_{ijk}^{(1)} &= \frac{\phi_{ijk}^{n}}{\sqrt{(\phi_{ijk}^{n})^2/\epsilon + (1-(\phi_{ijk}^{n})^2/\epsilon)e^{-\epsilon\Delta t}}},\\
\phi_{ijk}^{(2)} &= \frac{\phi_{ijk}^{(1)}}{1-(g\Delta t/2)\phi_{ijk}^{(1)}},\\
\frac{\phi_{ijk}^{(3)} - \phi_{ijk}^{(2)}}{\Delta t} &= -\frac{(1+\Delta_h)^2}{2}(\phi_{ijk}^{(3)} + \phi_{ijk}^{(2)}),\\
\phi_{ijk}^{(4)} &= \frac{\phi_{ijk}^{(3)}}{1-(g\Delta t/2)\phi_{ijk}^{(3)}},\\
\phi_{ijk}^{n+1} &= \frac{\phi_{ijk}^{(4)}}{\sqrt{(\phi_{ijk}^{(4)})^2/\epsilon + (1-(\phi_{ijk}^{(4)})^2/\epsilon)e^{-\epsilon\Delta t}}}.
\end{aligned}$$

4. Numerical Experiments

4.1. Convergence Test

In order to verify the rate of convergence of the proposed method, we consider the evolution of ϕ on a unit sphere. An initial piece of data is

$$\phi(x,y,z,0) = 0.15 + 0.1\cos(2\pi x)\cos(2\pi y)\cos(2\pi z)$$

and a signed distance function for the unit sphere is

$$\psi(x,y,z) = \sqrt{x^2+y^2+z^2} - 1$$

on $\Omega = [-1.5, 1.5]^3$. We fix the grid size to $h = 0.125$ and vary $\Delta t = T/2, T/2^2, T/2^3, T/2^4$ for $T = 0.00025$ with $\epsilon = 0.25$, $\delta = 2.2\sqrt{3}h$, and $tol = \Delta t$. Table 1 shows the L^2-errors of $\phi(x, y, z, T)$ and convergence rates with $g = 0$. Here, the errors are computed by comparison with a reference numerical solution using $\Delta t = T/2^6$. It is observed that the method is second-order accurate in time. Note that we obtain the same result for $g = 1$.

Table 1. L^2-errors and convergence rates for $g = 0$.

Δt	$T/2$		$T/2^2$		$T/2^3$		$T/2^4$
L^2-error	5.445×10^{-3}		1.341×10^{-3}		2.862×10^{-4}		5.519×10^{-5}
Rate		2.02		2.22		2.37	

4.2. Pattern Formation on a Sphere

Unless otherwise stated, we take an initial piece of data as

$$\phi(x, y, z, 0) = 0.15 + \text{rand}(x, y, z),$$

where $\text{rand}(x, y, z)$ is a uniformly distributed random number between -0.1 and 0.1 at the grid points, and use $\epsilon = 0.25$, $h = 1$, $\Delta t = 0.1$, $\delta = 1.1\sqrt{3}h$, and $tol = 10^{-4}$.

For $g = 0$ and 1, Figures 1 and 2 show the evolution of $\phi(x, y, z, t)$ on a sphere with $\psi(x, y, z) = \sqrt{x^2 + y^2 + z^2} - 32$ on $\Omega = [-36, 36]^3$, respectively. Depending on the value of g, we have different patterns, such as striped (Figure 1) and hexagonal (Figure 2) [11]. Figure 3 shows the energy decay with $g = 0$ and 1, where the energy $\mathcal{E}(\phi)$ is defined by

$$\mathcal{E}(\phi) = \int_{\Omega_\delta} \left(\frac{1}{4}\phi^4 - \frac{g}{3}\phi^3 + \frac{1}{2}\phi \left(-\epsilon + (1 + \Delta)^2 \right) \phi \right) d\mathbf{x}.$$

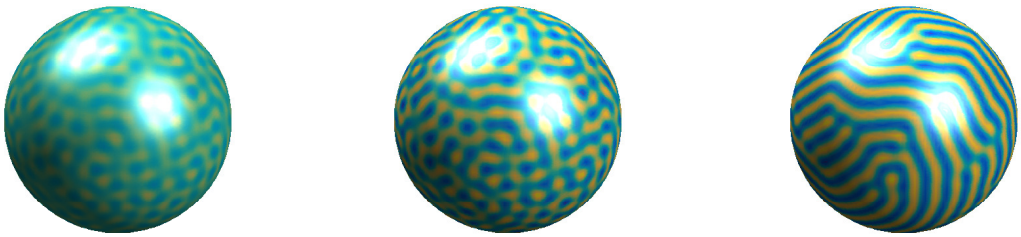

(**a**) $t = 12$ (**b**) $t = 20$ (**c**) $t = 100$

Figure 1. Evolution of $\phi(x, y, z, t)$ with $g = 0$. The yellow and blue regions indicate $\phi = 0.7540$ and -0.7783, respectively.

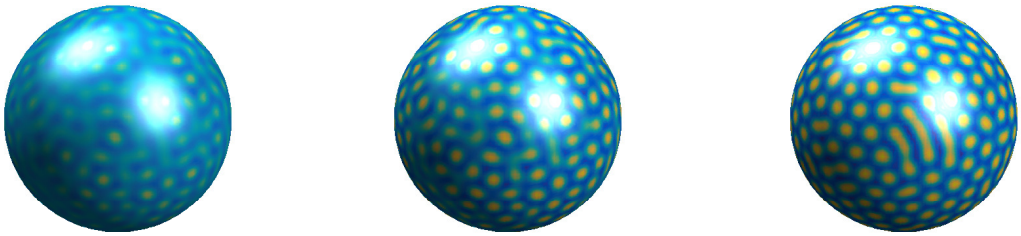

(**a**) $t = 12$ (**b**) $t = 16$ (**c**) $t = 100$

Figure 2. Evolution of $\phi(x, y, z, t)$ with $g = 1$. The yellow and blue regions indicate $\phi = 1.4320$ and -0.7152, respectively.

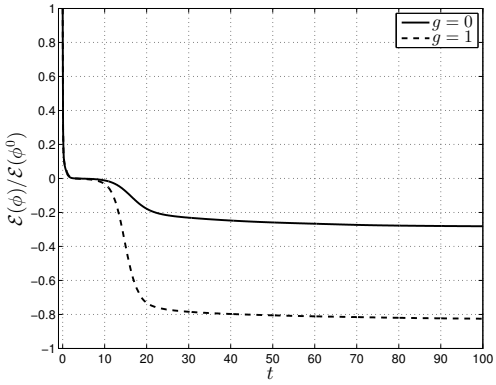

Figure 3. Evolution of $\mathcal{E}(\phi)/\mathcal{E}(\phi^0)$ on the sphere with $g = 0$ and 1.

4.3. Pattern Formation on a Sphere Perturbed by a Spherical Harmonic

In this section, we perform the evolution of ϕ on a sphere of center $(0, 0, 0)$ and radius 32 perturbed by a spherical harmonic $10\, Y_{10}^{7}(\theta, \varphi)$. Here, θ and φ are the polar and azimuthal angles, respectively, and the computational domain is $\Omega = [-40, 40]^3$. Figures 4 and 5 show the evolution of $\phi(x, y, z, t)$ with $g = 0$ and 1, respectively. From the results in Figures 4 and 5, we can see that our method can solve the SH type of equation on not only simple but also complex surfaces. Figure 6 shows the energy decay with $g = 0$ and 1.

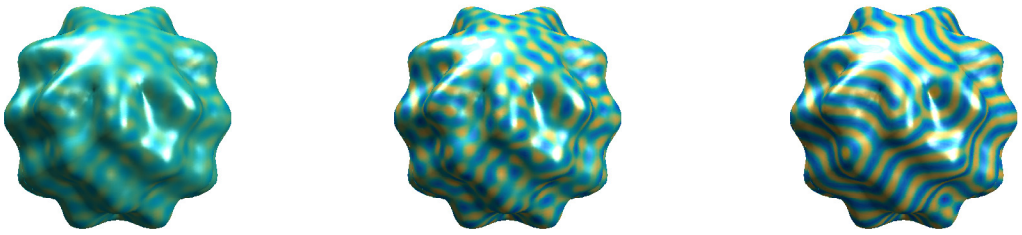

(**a**) $t = 12$ (**b**) $t = 20$ (**c**) $t = 100$

Figure 4. Evolution of $\phi(x, y, z, t)$ with $g = 0$. The yellow and blue regions indicate $\phi = 0.8717$ and -0.8372, respectively.

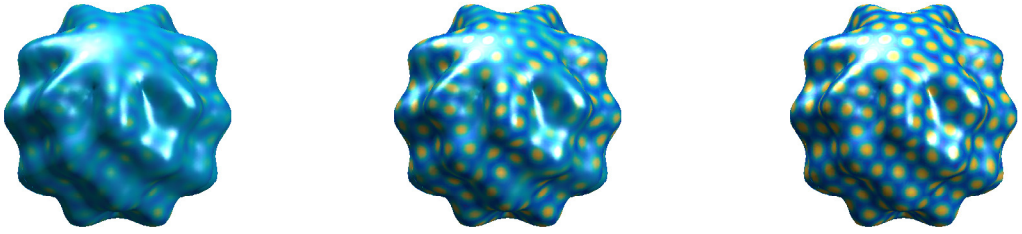

(**a**) $t = 12$ (**b**) $t = 16$ (**c**) $t = 100$

Figure 5. Evolution of $\phi(x, y, z, t)$ with $g = 1$. The yellow and blue regions indicate $\phi = 1.4833$ and -0.7135, respectively.

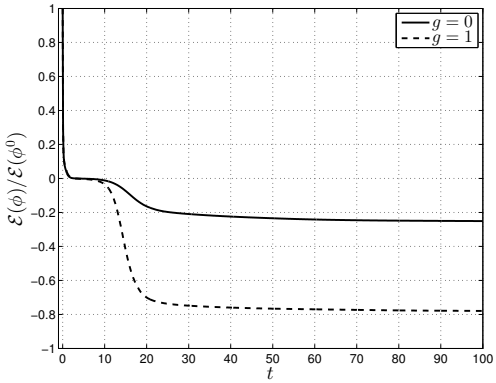

Figure 6. Evolution of $\mathcal{E}(\phi)/\mathcal{E}(\phi^0)$ on the perturbed sphere with $g = 0$ and 1.

4.4. Pattern Formation on a Spindle

Finally, we simulate the evolution of ϕ on a spindle that has narrow and sharp tips. The spindle is defined parametrically as

$$x = 16\cos\theta\sin\varphi, \quad y = 16\sin\theta\sin\varphi, \quad z = 32\left(\frac{2\varphi}{\pi} - 1\right),$$

where $\theta \in [0, 2\pi)$ and $\varphi \in [0, \pi)$, and the computational domain is $\Omega = [-20, 20] \times [-20, 20] \times [-36, 36]$. Figures 7 and 8 show the evolution of $\phi(x, y, z, t)$ with $g = 0$ and 1, respectively. The results in Figures 7 and 8 suggest that pattern formation on a surface having narrow and sharp tips can be simulated by using our method. Figure 9 shows the energy decay with $g = 0$ and 1.

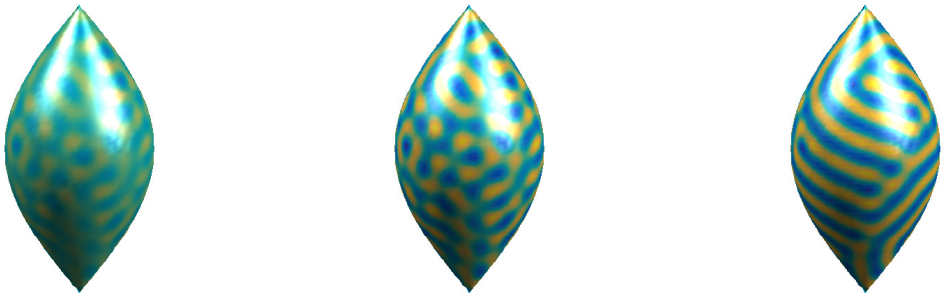

(**a**) $t = 12$ (**b**) $t = 20$ (**c**) $t = 100$

Figure 7. Evolution of $\phi(x, y, z, t)$ with $g = 0$. The yellow and blue regions indicate $\phi = 0.7059$ and -0.7593, respectively.

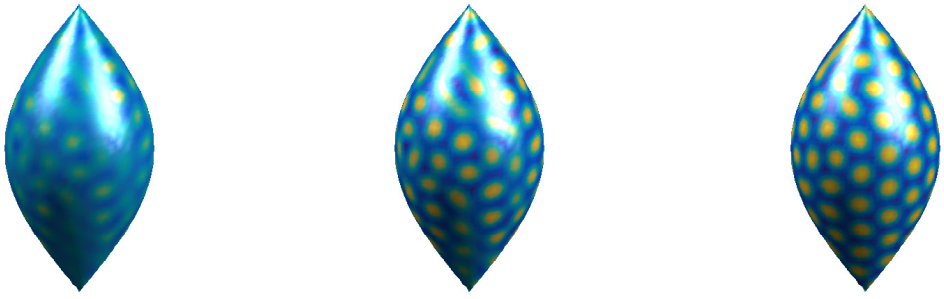

(**a**) $t = 12$ (**b**) $t = 16$ (**c**) $t = 100$

Figure 8. Evolution of $\phi(x, y, z, t)$ with $g = 1$. The yellow and blue regions indicate $\phi = 1.3842$ and -0.6224, respectively.

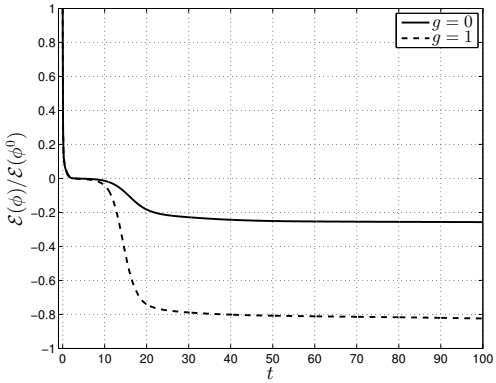

Figure 9. Evolution of $\mathcal{E}(\phi)/\mathcal{E}(\phi^0)$ on the spindle with $g = 0$ and 1.

5. Conclusions

We simulated pattern formation on surfaces numerically by solving the SH type of equation on surfaces by using the efficient linear second-order method. The method was based on the closest point and operator splitting methods and thus was easy to implement and linear. We confirmed that the proposed method gives the desired order of accuracy in time and observed that pattern formation on surfaces is affected by the value of g.

Funding: This work was supported by the Basic Science Research Program through the National Research Foundation of Korea (NRF) funded by the Ministry of Education (2019R1C1C1011112).

Acknowledgments: The corresponding author thanks the reviewers for the constructive and helpful comments on the revision of this article.

Conflicts of Interest: The author declares no conflict of interest.

References

1. Swift, J.; Hohenberg, P.C. Hydrodynamic fluctuations at the convective instability. *Phys. Rev. A* **1977**, *15*, 319–328. [CrossRef]
2. Hohenberg, P.C.; Swift, J.B. Effects of additive noise at the onset of Rayleigh–Bénard convection. *Phys. Rev. A* **1992**, *46*, 4773–4785. [CrossRef] [PubMed]
3. Cross, M.C.; Hohenberg, P.C. Pattern formation outside of equilibrium. *Rev. Mod. Phys.* **1993**, *65*, 851–1112. [CrossRef]
4. Rosa, R.R.; Pontes, J.; Christov, C.I.; Ramos, F.M.; Rodrigues Neto, C.; Rempel, E.L.; Walgraef, D. Gradient pattern analysis of Swift–Hohenberg dynamics: Phase disorder characterization. *Phys. A* **2000**, *283*, 156–159. [CrossRef]
5. Hutt, A.; Atay, F.M. Analysis of nonlocal neural fields for both general and gamma-distributed connectivities. *Phys. D* **2005**, *203*, 30–54. [CrossRef]
6. Cheng, M.; Warren, J.A. An efficient algorithm for solving the phase field crystal model. *J. Comput. Phys.* **2008**, *227*, 6241–6248. [CrossRef]
7. Wise, S.M.; Wang, C.; Lowengrub, J.S. An energy-stable and convergent finite-difference scheme for the phase field crystal equation. *SIAM J. Numer. Anal.* **2009**, *47*, 2269–2288. [CrossRef]
8. Gomez, H.; Nogueira, X. A new space–time discretization for the Swift–Hohenberg equation that strictly respects the Lyapunov functional. *Commun. Nonlinear Sci. Numer. Simul.* **2012**, *17*, 4930–4946. [CrossRef]
9. Elsey, M.; Wirth, B. A simple and efficient scheme for phase field crystal simulation. *ESAIM: Math. Model. Numer. Anal.* **2013**, *47*, 1413–1432. [CrossRef]
10. Sarmiento, A.F.; Espath, L.F.R.; Vignal, P.; Dalcin, L.; Parsani, M.; Calo, V.M. An energy-stable generalized-α method for the Swift–Hohenberg equation. *J. Comput. Appl. Math.* **2018**, *344*, 836–851. [CrossRef]
11. Lee, H.G. An energy stable method for the Swift–Hohenberg equation with quadratic–cubic nonlinearity. *Comput. Methods Appl. Mech. Eng.* **2019**, *343*, 40–51. [CrossRef]
12. Matthews, P.C. Pattern formation on a sphere. *Phys. Rev. E* **2003**, *67*, 036206. [CrossRef] [PubMed]

13. Sigrist, R.; Matthews, P. Symmetric spiral patterns on spheres. *SIAM J. Appl. Dyn. Syst.* **2011**, *10*, 1177–1211. [CrossRef]
14. Ruuth, S.J.; Merriman, B. A simple embedding method for solving partial differential equations on surfaces. *J. Comput. Phys.* **2008**, *227*, 1943–1961. [CrossRef]
15. Choi, Y.; Jeong, D.; Lee, S.; Yoo, M.; Kim, J. Motion by mean curvature of curves on surfaces using the Allen–Cahn equation. *Int. J. Eng. Sci.* **2015**, *97*, 126–132. [CrossRef]
16. Lee, H.G.; Kim, J. A simple and efficient finite difference method for the phase-field crystal equation on curved surfaces. *Comput. Methods Appl. Mech. Eng.* **2016**, *307*, 32–43. [CrossRef]
17. Pak, D.; Han, C.; Hong, W.-T. Iterative speedup by utilizing symmetric data in pricing options with two risky assets. *Symmetry* **2017**, *9*, 12. [CrossRef]
18. Zong, C.; Tang, Y.; Cho, Y.J. Convergence analysis of an inexact three-operator splitting algorithm. *Symmetry* **2018**, *10*, 563. [CrossRef]
19. Bertalmío, M.; Cheng, L.-T.; Osher, S.; Sapiro, G. Variational problems and partial differential equations on implicit surfaces. *J. Comput. Phys.* **2001**, *174*, 759–780. [CrossRef]
20. Greer, J.B. An improvement of a recent Eulerian method for solving PDEs on general geometries. *J. Sci. Comput.* **2006**, *29*, 321–352. [CrossRef]
21. Strang, G. On the construction and comparison of difference schemes. *SIAM J. Numer. Anal.* **1968**, *5*, 506–517. [CrossRef]